

Stream Query Denoising for Vectorized HD Map Construction

Shuo Wang^{1†} Fan Jia² Yingfei Liu² Yucheng Zhao² Zehui Chen¹
 Tiancai Wang² Chi Zhang² Xiangyu Zhang² Feng Zhao¹
¹University of Science and Technology of China ²MEGVII Technology

Abstract

To enhance perception performance in complex and extensive scenarios within the realm of autonomous driving, there has been a noteworthy focus on temporal modeling, with a particular emphasis on streaming methods. The prevailing trend in streaming models involves the utilization of stream queries for the propagation of temporal information. Despite the prevalence of this approach, the direct application of the streaming paradigm to the construction of vectorized high-definition maps (HD-maps) fails to fully harness the inherent potential of temporal information. This paper introduces the Stream Query Denoising (SQD) strategy as a novel approach for temporal modeling in high-definition map (HD-map) construction. SQD is designed to facilitate the learning of temporal consistency among map elements within the streaming model. The methodology involves denoising the queries that have been perturbed by the addition of noise to the ground-truth information from the preceding frame. This denoising process aims to reconstruct the ground-truth information for the current frame, thereby simulating the prediction process inherent in stream queries. The SQD strategy can be applied to those streaming methods (e.g., StreamMapNet) to enhance the temporal modeling. The proposed SQD-MapNet is the StreamMapNet equipped with SQD. Extensive experiments on nuScenes and Argoverse2 show that our method is remarkably superior to other existing methods across all settings of close range and long range. The code will be available soon.

1. Introduction

The High-Definition Map (HD-map) serves the crucial purpose of furnishing centimeter-level location information for map elements and plays a pivotal role in various applications within autonomous driving, including localization [22, 33, 34, 36, 39] and navigation [1, 2, 10]. Traditionally, the construction of HD-maps is conducted offline through SLAM-based methods [31, 41], which is both time-

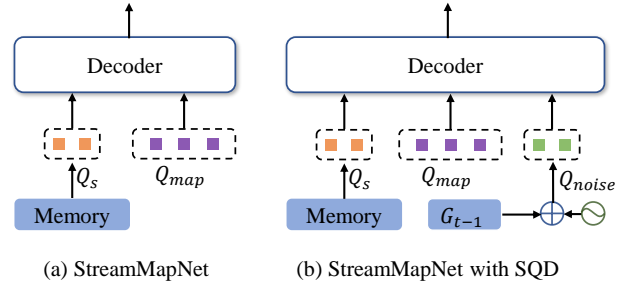


Figure 1. (a). The decoder process of StreamMapNet [38]. (b). StreamMapNet with the proposed stream query denoising (SQD). Purple blocks are global map queries learned by the network, orange blocks represent the stream queries from memory cache, and green blocks are the noised queries generated by adding noise to the ground truth G_{t-1} of previous frame $t - 1$.

consuming and labor-intensive. Recent research endeavors have shifted towards the construction of local maps within a predetermined range using onboard sensors. Although many existing works frame map construction as a semantic segmentation task [16, 23, 27, 30, 42], rasterized representations in such approaches exhibit redundant information, lack structural relationships between map elements, and often require extensive post-processing efforts [16]. In response to these limitations, MapTR [18] adopts an end-to-end approach to construct vectorized maps, akin to the DETR paradigm [4, 5, 21, 43].

Nevertheless, the aforementioned methods overlook the incorporation of temporal information. The efficacy of propagating sparse queries (hidden states) from the previous frame to the current frame has been demonstrated in temporal multi-view 3D object detection [20, 32]. While recent approaches grounded in vectorized representations share a similar paradigm with object detection, the direct application of the aforementioned temporal methods is not warranted due to inherent modeling variability between curves and bounding boxes. In the context of object detection, determining the speed of the ego and surrounding objects enables the prediction of their positions at the next timestamp. This stands in contrast to scenarios involving lines, where changes over time result in new parts appearing and

† Work done was during the internship at MEGVII Technology.

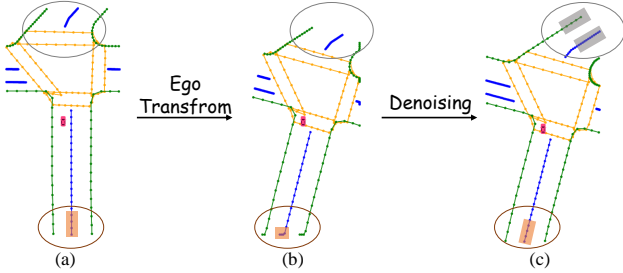


Figure 2. (a) shows the ground truth of previous frame. (b) is the transformation of (a) to current frame according to ego motion. (c) is the ground truth of current frame.

old parts detaching from the line, presenting a distinctive challenge not encountered in object detection.

Suppose the model’s predictions at the preceding moment precisely match the ground truth, and this valuable information is propagated to the current moment for improved initialization. Owing to ego-motion, the predictions must undergo transformation based on the matrix representing the transition between two frames. As depicted in Fig. 2, (a) and (b) illustrate the curves before and after transformation, respectively. The gray segment signifies the newly added part of the curve, necessitating all points along the entire line to acquire distinct offsets to accommodate the curve’s growth. Simultaneously, due to alterations in the perceptual range between the two frames, numerous points from the prior frame are truncated to the boundary of the current range, as depicted in the orange portion of Fig. 2. Points in this segment must assimilate different biases despite originating from nearly the same boundary. Clearly, explicitly teaching a network to grasp such intricate and diverse changes poses a challenge, and the temporal learning process for a network runs counter to conventional training.

To address the aforementioned challenges, we propose a novel approach called Stream Query Denoising (SQD) for the streaming model, exemplified by StreamMapNet [38], in the context of HD-map construction. Illustrated in Fig. 1 (a), StreamMapNet utilizes stream queries as hidden states for propagating temporal information. Our SQD strategy is designed to facilitate the learning of temporal consistency among map elements. The denoising process, involving the addition of noise to G_{t-1} to generate noise queries and subsequent reconstruction to simulate the prediction process of stream queries, is depicted in Fig. 1 (b). The SQD strategy consists of two main components. First, we introduce normal query denoising, considering three distinct noise strategies for curves: line shifting, angular rotation, and scale transformation. The acquisition of noise queries tailored for map elements is further explored. Second, for stream query denoising, we incorporate temporal adaptive matching to establish an explicit one-to-one correspondence between historical ground truths and current ones. To address warped errors inherent in temporal and current elements, a

dynamic query noising mechanism is devised.

In summary, the primary contributions of this paper are outlined as follows:

- The exploration of normal query denoising for HD-map construction, marking the first instance of such investigation. This encompasses three distinct noise strategies tailored for curves, accompanied by a detailed exploration of the methodology for acquiring noise queries.
- We propose the strategy of stream query denoising to assist the streaming model learn the temporal consistency of map elements.
- The development of SQD-MapNet, integrating our SQD strategy into StreamMapNet. Results showcase its notable superiority over state-of-the-art methods on existing benchmarks in both original and novel settings, underscoring the effectiveness of our proposed approach.

2. Related Works

2.1. Online Vectorized HD-Map Construction

There has been a surge of interest in leveraging onboard sensors for the construction of vectorized local HD-maps. HDMaNet [16] employs a semantic map prediction approach, followed by the aggregation of pixel-wise segmentation results through post-processing. In an effort to mitigate redundant information and alleviate the need for time-consuming post-processing, VectorMapNet [24] introduces a refinement step for map elements using an auto-regressive transformer. MapTR [18] adopts hierarchical queries and a fixed number of points to represent the map, while BeMapNet [29] utilizes piecewise Bezier curves to model map elements. Additionally, PivotNet [7] presents a map construction method based on pivot-based representations.

2.2. Temporal Camera-based Perception

The significance of temporal information is paramount, especially in intricate scenarios involving long distances, occlusion, and the like. Notably, the utilization of temporal information has been a focal point in the domain of camera-based 3D object detection. Approaches such as BEVDet4D [12] and BEVFormer v2 [37] adopt the strategy of stacking features from multiple historical frames and processing them in a single forward pass. However, this method incurs substantial computational costs and imposes limitations on the number of historical frames that can be effectively utilized. In contrast, VideoBEV [9] incorporates a recurrent long-term fusion module to sequentially fuse BEV features in a video stream. StreamPETR [32] and Sparse4D v2 [20] introduce the streaming queries strategy to propagate temporal information. Notably, StreamMapNet [38] extends this core idea to the construction of HD-Map by applying streaming queries and streaming BEV features.

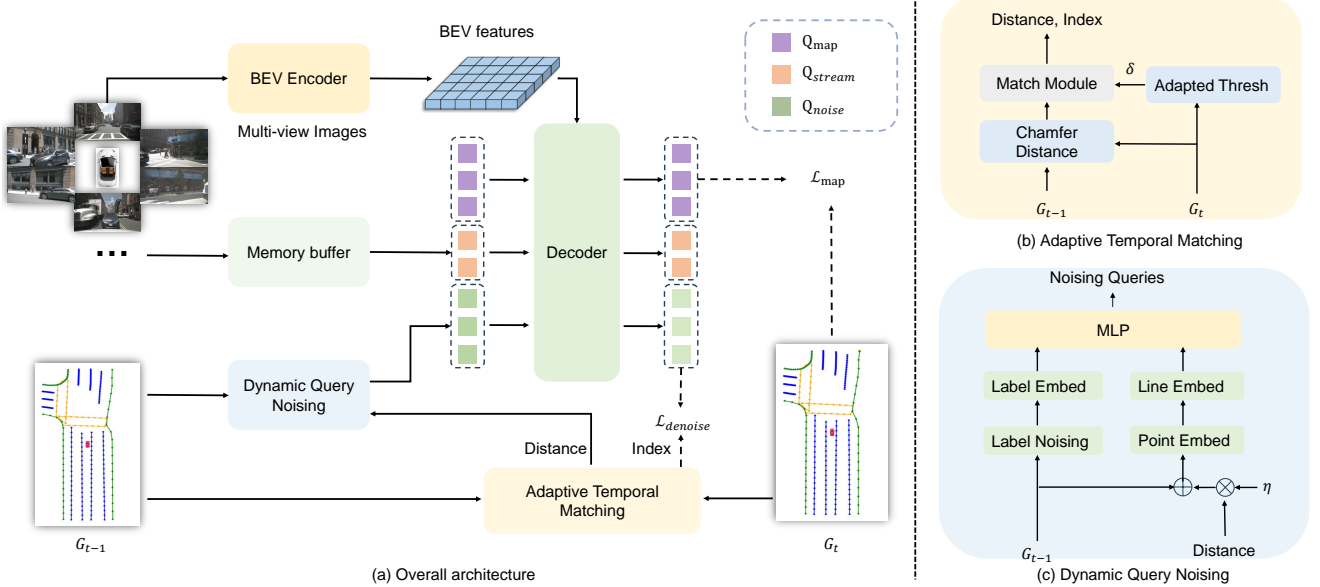


Figure 3. (a) shows the overall framework of SQR-MapNet. (b) and (c) are the specific implementations of adaptive temporal matching and dynamic query noising, respectively. G_{t-1} is the ground-truth of the last frame $t - 1$.

2.3. Query Denoising

DN-DETR [14] pioneers the utilization of query denoising to address the instability inherent in bipartite graph matching. DINO [40] extends this concept by introducing a definition of negative samples based on DN-DETR. Furthering this approach, MaskDINO [15] performs object detection and segmentation tasks concurrently. DN-MOT [8] tailors a denoising strategy to mitigate the impact of occlusion in multiple object tracking. In the context of this paper, we introduce the concept of stream query denoising for temporal HD-map construction. To the best of our knowledge, this is the first instance where the efficacy of query denoising in the temporal modeling of HD-map construction has been systematically examined.

3. Methodology

We first review the pipeline of StreamMapNet, followed by an exploration of normal query denoising. Subsequently, we introduce our approach to stream query denoising, elucidating two specific modules: adaptive temporal matching and dynamic query noising. The comprehensive architecture of our approach is illustrated in Fig. 3.

3.1. A Review of StreamMapNet

The overall pipeline of StreamMapNet consists of three primary components as follows:

BEV Feature Encoder. Given multi-view images from the onboard cameras, a shared backbone is employed to extract image features. Then these features are aggregated and processed by a Feature Pyramid Network [19] (FPN). Finally,

various PV2BEV transformation methods [17, 28] can be applied to obtain the BEV feature. Without loss of generality, we adapt the way of BEVFormer [17] in this work.

Polyline Decoder. Similar to most works [7, 18, 24], StreamMapNet views the vectorized map construction as a set prediction task and utilizes an end-to-end decoder [4] to extract lines from the BEV features, *i.e.*, the module takes the BEV feature and a set of learnable instance queries $\{Q_m\}_{m=1}^M$, and outputs a set of point descriptors $\{D_m\}_{m=1}^M$, where m is the max number of instances. Specifically, queries first perceive the global scene through global attention. Then each query generates n reference points, where n denotes the number of points forming a curve. Next, multi-point deformable attention of queries is performed on the dense BEV feature. Finally, we can obtain the final position of point descriptors $D_m = \{p_1^m, p_2^m, \dots, p_n^m\}$.

Temporal Query Propagation. Due to the static nature of map elements, there is a high probability that the instance at the current moment will continue to appear at the next moment, which means that the queries at present can provide a better reference position for the next moment than global initialization. StreamMapNet adopts the query propagation and BEV fusion to perform temporal fusion. Concretely, for query propagation, queries with the highest k scores as Q_{t-1} at the current frame are selected and the corresponding predicted reference points P_{t-1} can be obtained. Considering the movement of the ego, it utilizes the transformation matrix T between the coordinate systems of two frames

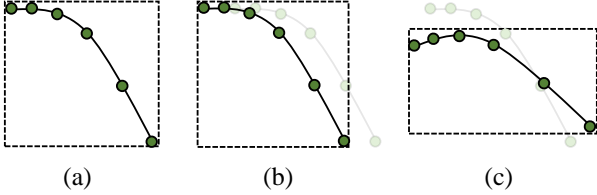


Figure 4. (a) is the original curve, which consists of a number of points and is surrounded by the minimum bounding rectangle. (b) and (c) shows box shifting and box scaling, respectively. The light-colored curves indicate the curves before noise addition.

before propagation as

$$Q'_t = \phi_t(\text{Concat}(Q_{t-1}, \text{Flatten}(T))) + Q_{t-1} \quad (1)$$

$$P'_t = T \cdot P_{t-1} \quad (2)$$

To this end, Q'_t and P'_t can be propagated to the next frame. Moreover, StreamMapNet employs a Gated Recurrent Unit [6] (GRU) to fuse these temporal BEV features.

3.2. Normal Query Denoising

The DETR series [4, 21, 43] faces challenges stemming from the instability of bipartite graph matching, leading to slow convergence and suboptimal results. Addressing these issues, DN-DETR [14] introduces the strategy of query denoising, effectively mitigating the aforementioned problems. However, as bounding boxes and curves exhibit inherent differences, the direct application of DN-DETR to the context of HD-map construction is not feasible. Consequently, we propose a novel approach termed normal query denoising. In this regard, we initially explore noise strategies tailored for curves. Subsequently, we detail the methodology for acquiring noise queries specific to HD-map construction.

3.2.1 Noise Strategies for Curves

A pivotal aspect of the denoising process hinges on the design of the noise, and to date, no prior work has delved into noise strategies tailored for curves. In this section, we examine three distinct noise strategies for curves: *line shifting*, *angular rotation*, and *scale transformation*. Here, line shifting and angular rotation refer to the global translation and rotation of the curve, respectively, while scale transformation pertains to the scaling of the curve’s length.

Inspired by the principles of DN-DETR [14], we introduce a novel approach that unifies the characterization of curves and bounding boxes for the first time. We propose a simple yet effective method for incorporating the three aforementioned noise types. Specifically, we encapsulate the curve by considering its minimum bounding rectangle as an instance representation, as depicted in Fig. 4 (a). Assuming x and y represent the center coordinates of the bounding box, and w and h denote the corresponding

width and height, the noise strategies for curves can be implemented in two distinct ways.

1) *Box shifting*: we introduce a random shift $(\Delta x, \Delta y)$ to the box, subject to the constraint $|\Delta x| < \frac{\lambda_1 w}{2}$ and $|\Delta y| < \frac{\lambda_2 h}{2}$, where λ_1, λ_2 are the maximum scale of noise. The position of the points in the curve with respect to the bounding box remains unchanged. This achieves the effect of *line shifting*, as illustrated in Fig. 4 (b). 2) *Box scaling*: We randomly sample the height and width within the intervals $[(1 - \lambda_3)h, (1 + \lambda_3)h]$ and $[(1 - \lambda_4)w, (1 + \lambda_4)w]$, respectively, where λ_3 and λ_4 denote the maximum scale of noise. Despite alterations in the angle and length of the curve, the relative positions of the points with respect to the box remain unchanged. Consequently, this approach achieves *angular rotation* and *scale transformation* simultaneously, as depicted in Fig. 4 (c).

3.2.2 Acquisition of Noising Query

Given a noisy curve, its category and point sets are denoted as cls and $\{p_1^m, p_2^m, \dots, p_n^m\}$, where m is the index of the curve and n is the number of points forming an instance. A learnable embedding is set for each category and then we can acquire the content embedding $C_q \in \mathbb{R}^{\frac{D}{2}}$, where D is the dimension of decoder embedding. For a point $p_i^m = \{x_i^m, y_i^m\}$, its position embedding can be generated by

$$P_i^m = \text{MLP}^{(pt)}(\text{Concat}(\text{PE}(x_i^m), \text{PE}(y_i^m))). \quad (3)$$

In our implementations, the positional encoding function PE maps a float to a vector with $\frac{D}{4}$ dimensions as: $\text{PE}: \mathbb{R} \rightarrow \mathbb{R}^{\frac{D}{4}}$, and the function $\text{MLP}^{(pt)}$ projects a $\frac{D}{2}$ dimensional vector into $\frac{D}{2}$ dimensions: $\text{MLP}^{(pt)}: \mathbb{R}^{\frac{D}{2}} \rightarrow \mathbb{R}^{\frac{D}{2}}$. Then the position embedding of the instance can be obtained as

$$Pos_q = \text{MLP}^{(pos)}(\text{Concat}(P_1^m, P_2^m, \dots, P_n^m)), \quad (4)$$

where $\text{MLP}^{(pos)}: \mathbb{R}^{\frac{nD}{2}} \rightarrow \mathbb{R}^{\frac{D}{2}}$ fuses the information from all the points into the position information of the curve.

Since we use deformable attention to interact the queries with the reference points for information, we acquire the denoising query $Q_{denoise}$ by fusing the content information with the position information via $\text{MLP}^{(fuse)}: \mathbb{R}^D \rightarrow \mathbb{R}^D$ as

$$Q_{denoise} = \text{MLP}^{(fuse)}(\text{Concat}(C_q, Pos_q)), \quad (5)$$

3.3. Stream Query Denoising

Query denoising (DN) [14] has demonstrated its efficacy in improving the network’s ability to model queries. However, as illustrated in Fig. 2, the intricate nature of predictions generated by streaming queries introduces challenges when adding noise to the current ground truth. This complexity

arises from the difficulty in simulating both the increasing and decreasing parts of previously predicted curves. To address this, we introduce Stream Query Denoising (SQD), a novel approach that involves adding noise to the ground truth of the previous frame to emulate the predictions made by streaming queries. Moreover, considering that a portion of curves in the previous ground truth remains unchanged due to ego-motion, adding noise to the ground truth of the previous frame is tantamount to DN. Therefore, SQD not only facilitates the network in learning to model temporal queries and current queries simultaneously but also aligns with the principles of DN, making it a versatile strategy for enhancing the network’s temporal understanding. Next, we will introduce two essential components, namely adaptive temporal matching and dynamic query noising, to effectively complement and enhance the Stream Query Denoising (SQD) strategy.

3.3.1 Adaptive Temporal Matching

In the process of stream query denoising, we have no access to an explicit one-to-one correspondence between temporal ground truth and current ones. In order to circumvent the instability associated with bipartite graph matching, we propose Adaptive Temporal Matching (ATM).

Let $\{y_1^{t-1}, y_2^{t-1}, \dots, y_m^{t-1}\}$ and $\{y_1^t, y_2^t, \dots, y_n^t\}$ represent the ground truth in the previous frame and the current frame, respectively. Here, y is composed of a fixed number of points, and m and n denote the number of points in the respective ground truth. Due to the movement of the ego, the transformation matrix T between the coordinate systems of the two frames is employed to convert $\{y_1^{t-1}, y_2^{t-1}, \dots, y_m^{t-1}\}$ to $\{\hat{y}_1^{t-1}, \hat{y}_2^{t-1}, \dots, \hat{y}_m^{t-1}\}$. For each curve in the current frame y_i^t , we compute the Chamfer distance (CD) between it and each instance in the previous frame. The minimum distance and its corresponding location are preserved::

$$\text{CD}_{Dir}(S_1, S_2) = \frac{1}{S_1} \sum_{p \in S_1} \min_{q \in S_2} \|p - q\|_2, \quad (6)$$

$$\text{CD}(S_1, S_2) = \text{CD}_{Dir}(S_1, S_2) + \text{CD}_{Dir}(S_2, S_1), \quad (7)$$

$$D, idx = \min_{j \in [1, m]} (\text{CD}(y_i^t, \hat{y}_j^{t-1})), \quad (8)$$

where CD_{Dir} is the directional Chamfer distance and CD is the bi-directional Chamfer distance; S_1 and S_2 are the two sets of points on the curves; idx denotes the index closest to the curve itself and D is the minimum distance value.

Due to the inherent differences in the properties of each curve, a unique tolerance threshold is set for each instance. Initially, we extract the maximum bounding rectangle from the curve and consider the width w and height h of the rectangle as the reference scale for this curve. Subsequently,

the threshold is calculated as:

$$\delta = \alpha \frac{w + h}{2}, \quad (9)$$

where α is the degree of the tolerance.

Only when the minimum distance in Eq. (8) is less than the threshold of the corresponding instance in the current frame, we will assign the temporal instance to the current curve. Consequently, through Adaptive Temporal Matching (ATM), we establish the correspondence between the temporal ground truth and the current one.

3.3.2 Dynamic Query Noising

Upon transforming the ground truth of the previous frame into the current frame based on ego-motion, a natural bias emerges between it and the ground truth in the current frame. Perturbing all ground truths equally, without considering the instance’s inherent noise, is suboptimal. To address this, we introduce Dynamic Query Noising.

After obtaining the matching relation in Sec. 3.3.1, the corresponding minimum Chamfer distance D can also be derived from Eq. (8). Subsequently, the decay rate of noise for each instance can be calculated as follows:

$$R_{decay} = 1 - \frac{D}{\gamma \cdot \frac{\delta}{\alpha}}, \quad (10)$$

where γ is the predefined decay scale and δ is acquired by Eq. (9).

To illustrate, considering the box-level scale in Sec. 3.2.1 as an example, if we assume that the randomly added noise is $\eta = \{\Delta x, \Delta y, \Delta w, \Delta h\}$, then the final instance is represented as

$$B_{ins} = \{x, y, w, h\} + \{\Delta x, \Delta y, \Delta w, \Delta h\} \cdot R_{decay}, \quad (11)$$

where $\{x, y, w, h\}$ is the original instance.

After getting the noisy categories and point sets, we derive the noising queries according to Sec. 3.2.2.

3.3.3 Objective Function

Our model adopts an end-to-end training approach. During training, we employ the same map loss function as StreamMapNet[38], including the classification loss \mathcal{L}_{Focal} , the line loss \mathcal{L}_{line} and the translation loss \mathcal{L}_{trans} .

$$\mathcal{L}_{map} = \lambda_1 \mathcal{L}_{Focal} + \lambda_2 \mathcal{L}_{line} + \lambda_3 \mathcal{L}_{trans}, \quad (12)$$

where λ_1, λ_2 and λ_3 are hyperparameters.

Additionally, for the prediction results of denoising queries, we use the same type of classification loss and line loss to construct $\mathcal{L}_{denoise}$.

$$\mathcal{L}_{denoise} = \lambda_4 \mathcal{L}_{Focal}^{DN} + \lambda_5 \mathcal{L}_{line}^{DN}, \quad (13)$$

where \mathcal{L}_{Focal}^{DN} and \mathcal{L}_{line}^{DN} are classification loss and the line loss of the denoising predictions and λ_4, λ_5 are hyperparameters.

Finally, the overall loss is defined as:

$$\mathcal{L}_{train} = \mathcal{L}_{map} + \mathcal{L}_{denoise} \quad (14)$$

4. Experiments

4.1. Experimental Settings

Datasets. We evaluate SQD-MapNet on two competitive and large-scale datasets, *i.e.*, nuScenes [3] and Argoverse2 [35]. The nuScenes dataset is annotated with 2Hz and each sample comprises 6 synchronized cameras. The Argoverse2 is annotated with 10Hz. Each frame contains 7 ring cameras and 2 stereo cameras. We adopt images from the ring cameras only and unify the frame rate of the dataset to 2Hz following the implementation in [7, 38].

Evaluation Metrics. For the sake of fair comparison, we focus on 3 static map categories, namely *lane-divider*, *ped-crossing*, and *road-boundary*. We evaluate the models on both small perceptual range (30m front and back, 15m left and right) and larger perceptual range (50m front and back, 25m left and right). The distinct thresholds to calculate the AP is set to $\{0.5m, 1.0m, 1.5m\}$ for the 30m range, and $\{1.0m, 1.5m, 2.0m\}$ for the 50m range.

Implementation Details. We adopt ResNet-50 [11] as backbones and use BEVFormer [17] with a single encoder layer for BEV feature extraction. The sizes of BEV feature map are $100 \times 50 m$ for the small perceptual range and $200 \times 100 m$ for the larger range. The strategy of streaming training is consistent with StreamMapNet [38]. During the single-frame training phase, we adopt the normal query denoising instead of stream query denoising. All models are trained for 24 epochs on the nuScenes dataset and 30 epochs on Argoverse 2 dataset. We adopt AdamW optimizer [25] with a learning rate of 5×10^{-4} . All experiments are conducted on 8 NVIDIA Telsa V100 GPUs with a batch size of 32.

4.2. Comparisons with State-of-the-arts

Performance on nuScenes. We first compare the proposed SQD-MapNet with previous competitive vision-based counterparts on the nuScenes validation set for both 30m and 50m perception ranges. As shown in Tab. 1, SQD-MapNet outperforms existing approaches under different perceptual range settings by a significant margin. Specifically, SQD-MapNet achieves 63.9 and 64.0 mAP within only 24 epochs under the short- and long-range evaluation settings, surpassing the previous state-of-the-art method, StreamMapNet, by more than 3.0 mAP. Notably, armed with the strong V2-99 [13] backbone pretrained on DD3D [26], our SQD-MapNet achieves 74.0 and 75.2 mAP,

setting new state-of-the-art for the competitive nuScenes benchmark. We also provide the results on the new split of the dataset adopted in StreamMapNet [38] in the *supplementary material*.

Performance on Argoverse2. In addition to the widely-adopted nuScenes dataset, we also gauge SQD-MapNet on the large-scale dataset Argoverse2 [35] to further validate the effectiveness of our approach. To keep consistent with the evaluation protocol in nuScenes dataset, we report the results for both $60 \times 30 m$ and $100 \times 50 m$ ranges. As shown in Tab. 2, SQD-MapNet consistently outperforms StreamMapNet by about 2.0 mAP, validating the generalization and superiority of our approach. For the new split of dataset adopted by StreamMapNet [38], we additionally show the results in the *supplementary material*.

4.3. Ablation Study

In this section, we provide extensive ablation studies to explore the effectiveness of main components in SQD-MapNet, providing a deeper understanding of our approach. If not specified, all experiments are conducted on nuScenes dataset at a perceptual range of $60 \times 30 m$.

Main Ablations To understand how each component contributes to the final performance, we subsequently add the proposed modules to our baseline and report the performance in Tab. 3. We regard StreamMapNet [38] without temporal streaming as the vanilla baseline. When applying the streaming strategy proposed by [38], the performance declines by 0.7 mAP, indicating that it is difficult for the network to learn the constant changes in curves of different frames. Then we add the dynamic query noising mechanism in the training process, the mAP is improved by a large margin (3.7 mAP). Additionally, when adaptive temporal matching is applied, we observe a further 1.0 improvement, which verifies the necessity of the matching strategy. Overall, the performance of SQD-MapNet achieves 63.9 mAP, yielding a performance enhancement of 4.0 mAP.

Ways for Adaptive Temporal Matching Tab. 4 ablates the performance of different matching ways and matching scales on SQD-MapNet. Concretely, α denotes the value of adaptive matching scale and β is the predefined fixed matching threshold. Due to the ignorance of the curve’s properties, a fixed threshold only yields a maximum score of 62.8 mAP. When α is small, the result is not optimal, suggesting that strict matching may cause some ground truths to be filtered out during the denoising process. As the value of α increases, which means the tolerance level of transformation bias becomes larger, more positive samples of the previous frame can be matched. Specifically, the performance reaches 63.5 mAP when α equals 0.1. However, when α keeps increasing, the detection accuracy starts to incline, indicating that there are plenty of noisy samples from the previous frames incorrectly matched with ground truths at

Range	Method	Backbone	Image Size	Epoch	AP_{ped}	AP_{div}	AP_{bound}	mAP
$60 \times 30 m$	VectorMapNet [24]	R50	256×480	110	36.1	47.3	39.3	40.9
	MapTR [18]	R50	480×800	24	46.3	51.5	53.1	50.3
	BeMapNet [29]	R50	512×896	30	57.7	62.3	59.4	59.8
	PivotNet [7]	R50	-	24	56.2	56.5	60.1	57.6
	StreamMapNet [38]	R50	480×800	24	60.4	61.9	58.9	60.4
	SQD-MapNet (Ours)	R50	480×800	24	63.0	62.5	63.3	63.9
	StreamMapNet [†] [38]	R50	480×800	24	-	-	-	62.9
	SQD-MapNet [†] (Ours)	R50	480×800	24	63.6	66.6	64.8	65.0
SQD-MapNet (Ours)	V2-99	900×1600	110	74.2	72.3	75.6	74.0	
$100 \times 50 m$	MapTR [18]	R50	480×800	24	45.5	47.1	43.9	45.5
	StreamMapNet [38]	R50	480×800	24	62.9	63.1	55.8	60.6
	SQD-MapNet (Ours)	R50	480×800	24	67.0	65.5	59.5	64.0
	SQD-MapNet (Ours)	V2-99	900×1600	110	75.5	74.9	75.2	75.2

Table 1. Comparison with SOTAs on nuScenes [3] at both $30 m$ and $50 m$ ranges. The [†] indicates that we have added tricks such as dcn and SyncBN to align with experimental setups of StreamMapNet [38]. We reproduce the results of MapTR [18] and BeMapNet [29] under the setting of $100 \times 50 m$ with their public codes. The - means that no corresponding results were reported in the original paper.

Range	Method	Backbone	Image Size	Epoch	AP_{ped}	AP_{div}	AP_{bound}	mAP
$60 \times 30 m$	HDMaNet [16]	Effi-B0	-	-	13.1	5.7	37.6	18.8
	VectorMapNet [24]	R50	-	-	38.3	36.1	39.2	37.9
	PivotNet [7]	R50	-	6	31.3	47.5	43.4	40.7
	StreamMapNet [38]	R50	608×608	30	62.0	59.5	63.0	61.5
	SQD-MapNet (Ours)	R50	608×608	30	64.9	60.2	64.9	63.3
$100 \times 50 m$	VectorMapNet [24]	R50	384×384	120	-	-	-	30.2
	MapTR [18]	R50	608×608	30	-	-	-	47.5
	StreamMapNet [38]	R50	608×608	30	-	-	-	57.7
	SQD-MapNet (Ours)	R50	608×608	30	66.9	54.9	56.1	59.3

Table 2. Performance comparison of various methods on Argoverse 2 [35] at both $30 m$ and $50 m$ ranges. - means that no corresponding results were reported in the original paper. The results of VectorMapNet [24] and MapTR [18] in $100 \times 50 m$ are directly borrowed from StreamMapNet [38]. Since PivotNet [7] trains the model on the full training set, we reimplement it by training with the same number of iterations for a fair comparison.

Method	mAP
Single-frame baseline	59.9
+ Temporal Stream	59.2 (-0.7)
+ Dynamic Query Noising	62.9 (+3.7)
+ Adaptive Temporal Matching	63.9 (+1.0)

Table 3. Ablations on each component in SQD-MapNet. Starting from a single-frame baseline to the final model.

the current frame.

Decay Rate of Noise After warping the previous frame curve to the current frame, there is a natural noise between the previous one and the current ground truth. Besides, we add extra random noise during the dynamic query noising phase. Therefore, deciding the right level of decay rates of the added noise is non-trivial. We experiment SQD-MapNet with different γ in Tab. 5. From the table, we can conclude that a small ratio of 0.2 can balance both the learning diver-

Matching Scale	Adaptive Matching	mAP
$\beta = 2.5$	\times	62.0
$\beta = 4.0$	\times	62.3
$\beta = 5.0$	\times	62.8
$\alpha = 0.05$	\checkmark	63.0
$\alpha = 0.1$	\checkmark	63.5
$\alpha = 0.2$	\checkmark	62.9
$\alpha = 0.3$	\checkmark	63.0

Table 4. Comparison of matching ways and matching scale.

sity and the negative effect introduced by noise.

Normal and Stream Query Denoising We also compare the performance of our baseline, normal query denoising, and stream query denoising in Tab. 6. It shows that normal query denoising improves 3.5 mAP performance compared to the baseline. Stream query denoising further outperforms the normal query denoising by 1.2 mAP. The reasons can

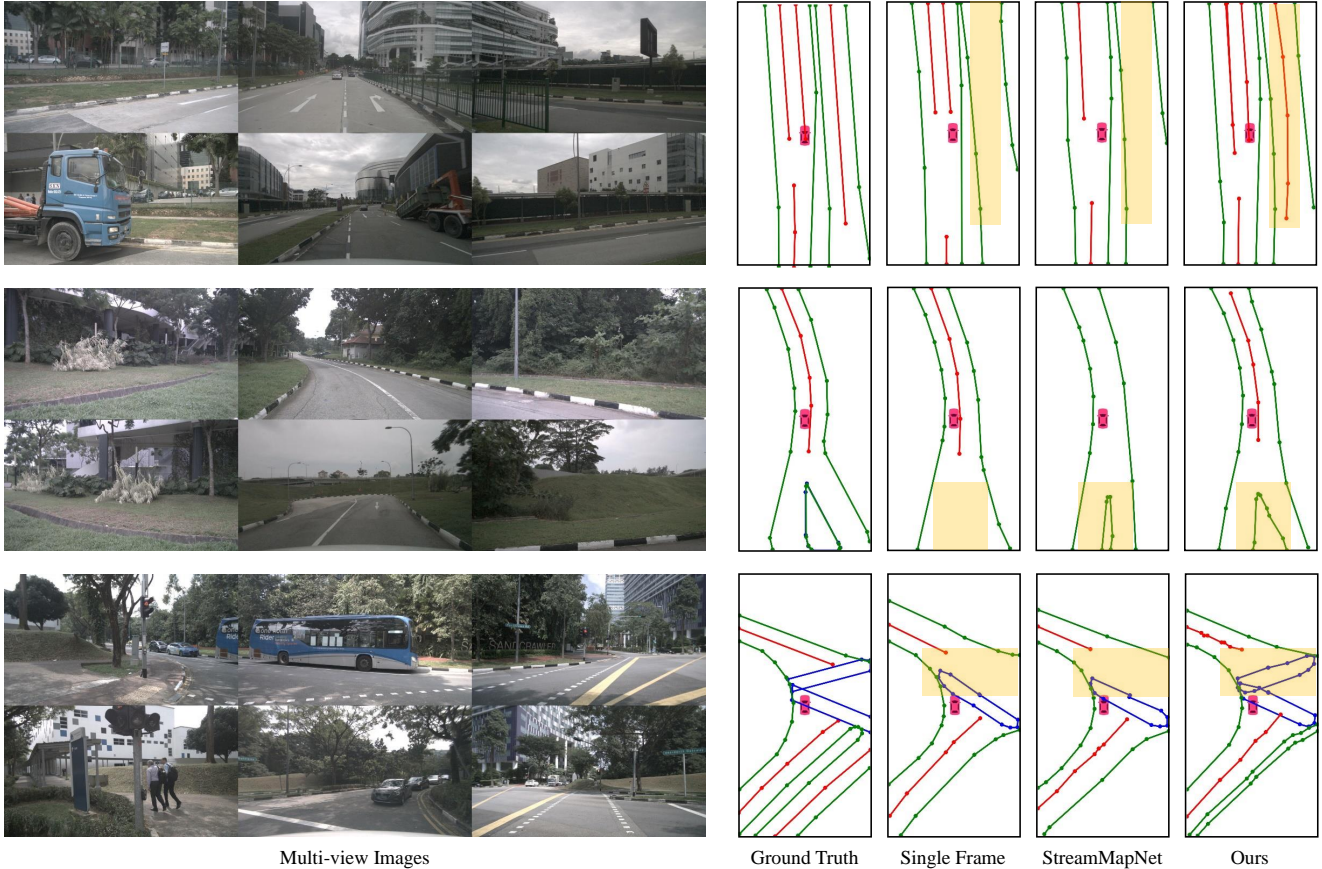


Figure 5. Comparison with the single-frame model and StreamMapNet [38] on qualitative visualization under different scenarios. In the HD-map, green lines denote *road boundaries*, red lines indicate *lane-dividers*, and blue lines denote *pedestrian crossings*.

Decay Rate	AP_{ped}	AP_{div}	AP_{bound}	mAP
$\gamma = 0.1$	62.5	65.3	62.5	63.4
$\gamma = 0.2$	63.0	65.5	63.3	63.9
$\gamma = 0.3$	59.0	64.1	63.8	62.3
$\gamma = 0.5$	59.7	65.8	63.7	63.0
$\gamma = 0.7$	61.7	64.0	61.3	62.4

Table 5. Effect of different decay rates of noise on the final results.

be two-fold: (i) A portion of temporal curves are identical to the ground truth of the current frame, so normal query denoising is sometimes equivalent to stream query denoising, which enhances the ability to model stream queries. (ii) stream query denoising helps the transformer decoder learn to exploit the stream queries by introducing temporal ground truth.

Way of Denoising	mAP
w/o Denoising	59.2
Normal Query Denoising	62.7
Stream Query Denoising	63.9

Table 6. Comparison of denoising and temporal denoising.

4.4. Qualitative Analysis

We show some qualitative comparisons with a single-frame model, StreamMapNet [38], and SQD-MapNet in Fig. 5. The single-frame model is reproduced with [38] without temporal information. We can find that the single-frame model and StreamMapNet easily fails to recognize some curves in both simple and complex scenes. Compared with other methods, SQD-MapNet utilizes the temporal information more effectively and accurately recognizes curves.

5. Conclusion

In this paper, we introduce the stream query denoising (SQD) strategy to enhance the temporal streaming modeling in HD-map construction. Such strategy is only applied during training process and can be removed for the inference. Extensive experiments on nuScenes and Argoverse2 show that the performance of streaming models (e.g., StreamMapNet) are greatly improved with the proposed SQD strategy. The resulting SQD-MapNet framework is remarkably superior to other existing methods across all settings of close range and long range.

Discussion: Our proposed SQD strategy greatly enhances the temporal modeling of HD-map construction, as verified on nuScenes and Argoverse2. However, the effectiveness of our method can only be verified based on streaming models. And there is only one streaming baseline StreamMapNet available at present, lacking of abundant verification. The temporal modeling on HD-map construction is quite important for autonomous driving. It can keep the temporal consistency and stability of predictions cross different frames. For example, temporal modeling can deal with the case where the confidence score of prediction is floated around the set threshold. Therefore, related researchers in the community are encouraged to explore more on the temporal modeling for HD-map construction. The temporal consistency, achieved by our adaptive temporal matching may provide some new insight for the community.

References

- [1] Morris Antonello, Marco Carraro, Marco Pierobon, and Emanuele Menegatti. Fast and robust detection of fallen people from a mobile robot. In *2017 IEEE/RSJ international conference on intelligent robots and systems (IROS)*, pages 4159–4166. IEEE, 2017. 1
- [2] Esmat Bekir. *Introduction to modern navigation systems*. World scientific, 2007. 1
- [3] Holger Caesar, Varun Bankiti, Alex H Lang, Sourabh Vora, Venice Erin Liang, Qiang Xu, Anush Krishnan, Yu Pan, Giancarlo Baldan, and Oscar Beijbom. nuscenes: A multi-modal dataset for autonomous driving. In *Proceedings of the IEEE/CVF conference on computer vision and pattern recognition*, pages 11621–11631, 2020. 6, 7
- [4] Nicolas Carion, Francisco Massa, Gabriel Synnaeve, Nicolas Usunier, Alexander Kirillov, and Sergey Zagoruyko. End-to-end object detection with transformers. In *European conference on computer vision*, pages 213–229. Springer, 2020. 1, 3, 4
- [5] Jiahao Chang, Shuo Wang, Hai-Ming Xu, Zehui Chen, Chenhongyi Yang, and Feng Zhao. Detrdistill: A universal knowledge distillation framework for detr-families. In *Proceedings of the IEEE/CVF International Conference on Computer Vision*, pages 6898–6908, 2023. 1
- [6] Junyoung Chung, Caglar Gulcehre, KyungHyun Cho, and Yoshua Bengio. Empirical evaluation of gated recurrent neural networks on sequence modeling. *arXiv preprint arXiv:1412.3555*, 2014. 4
- [7] Wenjie Ding, Limeng Qiao, Xi Qiu, and Chi Zhang. Pivotnet: Vectorized pivot learning for end-to-end hd map construction. In *Proceedings of the IEEE/CVF International Conference on Computer Vision*, pages 3672–3682, 2023. 2, 3, 6, 7
- [8] Teng Fu, Xiaocong Wang, Haiyang Yu, Ke Niu, Bin Li, and Xiangyang Xue. Denoising-mot: Towards multiple object tracking with severe occlusions. In *Proceedings of the 31st ACM International Conference on Multimedia*, pages 2734–2743, 2023. 3
- [9] Chunrui Han, Jianjian Sun, Zheng Ge, Jinrong Yang, Runpei Dong, Hongyu Zhou, Weixin Mao, Yuang Peng, and Xiangyu Zhang. Exploring recurrent long-term temporal fusion for multi-view 3d perception. *arXiv preprint arXiv:2303.05970*, 2023. 2
- [10] Ahmed M Hasan, Khairulmizam Samsudin, Abdul Rahman Ramli, RS Azmir, and SA Ismaeel. A review of navigation systems (integration and algorithms). *Australian journal of basic and applied sciences*, 3(2):943–959, 2009. 1
- [11] Kaiming He, Xiangyu Zhang, Shaoqing Ren, and Jian Sun. Deep residual learning for image recognition. In *Proceedings of the IEEE conference on computer vision and pattern recognition*, pages 770–778, 2016. 6
- [12] Junjie Huang and Guan Huang. Bevdet4d: Exploit temporal cues in multi-camera 3d object detection. *arXiv preprint arXiv:2203.17054*, 2022. 2
- [13] Youngwan Lee, Joong-won Hwang, Sangrok Lee, Yuseok Bae, and Jongyoul Park. An energy and gpu-computation efficient backbone network for real-time object detection. In *Proceedings of the IEEE/CVF conference on computer vision and pattern recognition workshops*, pages 0–0, 2019. 6
- [14] Feng Li, Hao Zhang, Shilong Liu, Jian Guo, Lionel M Ni, and Lei Zhang. Dn-detr: Accelerate detr training by introducing query denoising. In *Proceedings of the IEEE/CVF Conference on Computer Vision and Pattern Recognition*, pages 13619–13627, 2022. 3, 4
- [15] Feng Li, Hao Zhang, Huaizhe Xu, Shilong Liu, Lei Zhang, Lionel M Ni, and Heung-Yeung Shum. Mask dino: Towards a unified transformer-based framework for object detection and segmentation. In *Proceedings of the IEEE/CVF Conference on Computer Vision and Pattern Recognition*, pages 3041–3050, 2023. 3
- [16] Qi Li, Yue Wang, Yilun Wang, and Hang Zhao. Hdmapnet: An online hd map construction and evaluation framework. In *2022 International Conference on Robotics and Automation (ICRA)*, pages 4628–4634. IEEE, 2022. 1, 2, 7
- [17] Zhiqi Li, Wenhai Wang, Hongyang Li, Enze Xie, Chonghao Sima, Tong Lu, Yu Qiao, and Jifeng Dai. Bevformer: Learning bird’s-eye-view representation from multi-camera images via spatiotemporal transformers. In *European conference on computer vision*, pages 1–18. Springer, 2022. 3, 6
- [18] Bencheng Liao, Shaoyu Chen, Xinggang Wang, Tianheng Cheng, Qian Zhang, Wenyu Liu, and Chang Huang. Maptr: Structured modeling and learning for online vectorized hd map construction. *arXiv preprint arXiv:2208.14437*, 2022. 1, 2, 3, 7
- [19] Tsung-Yi Lin, Piotr Dollár, Ross Girshick, Kaiming He, Bharath Hariharan, and Serge Belongie. Feature pyramid networks for object detection. In *Proceedings of the IEEE conference on computer vision and pattern recognition*, pages 2117–2125, 2017. 3
- [20] Xuewu Lin, Tianwei Lin, Zixiang Pei, Lichao Huang, and Zhizhong Su. Sparse4d v2: Recurrent temporal fusion with sparse model. *arXiv preprint arXiv:2305.14018*, 2023. 1, 2
- [21] Shilong Liu, Feng Li, Hao Zhang, Xiao Yang, Xianbiao Qi, Hang Su, Jun Zhu, and Lei Zhang. Dab-detr: Dynamic

- anchor boxes are better queries for detr. *arXiv preprint arXiv:2201.12329*, 2022. 1, 4
- [22] Yingfei Liu, Tiancai Wang, Xiangyu Zhang, and Jian Sun. Petr: Position embedding transformation for multi-view 3d object detection. In *European Conference on Computer Vision*, pages 531–548. Springer, 2022. 1
- [23] Yingfei Liu, Junjie Yan, Fan Jia, Shuailin Li, Aqi Gao, Tiancai Wang, and Xiangyu Zhang. Petr_{v2}: A unified framework for 3d perception from multi-camera images. In *Proceedings of the IEEE/CVF International Conference on Computer Vision*, pages 3262–3272, 2023. 1
- [24] Yicheng Liu, Tianyuan Yuan, Yue Wang, Yilun Wang, and Hang Zhao. Vectormapnet: End-to-end vectorized hd map learning. In *International Conference on Machine Learning*, pages 22352–22369. PMLR, 2023. 2, 3, 7
- [25] Ilya Loshchilov and Frank Hutter. Fixing weight decay regularization in adam. 2018. 6
- [26] Dennis Park, Rares Ambrus, Vitor Guizilini, Jie Li, and Adrien Gaidon. Is pseudo-lidar needed for monocular 3d object detection? In *Proceedings of the IEEE/CVF International Conference on Computer Vision*, pages 3142–3152, 2021. 6
- [27] Lang Peng, Zhirong Chen, Zhangjie Fu, Pengpeng Liang, and Erkang Cheng. Bevsegformer: Bird’s eye view semantic segmentation from arbitrary camera rigs. In *Proceedings of the IEEE/CVF Winter Conference on Applications of Computer Vision*, pages 5935–5943, 2023. 1
- [28] Jonah Philion and Sanja Fidler. Lift, splat, shoot: Encoding images from arbitrary camera rigs by implicitly unprojecting to 3d. In *Computer Vision—ECCV 2020: 16th European Conference, Glasgow, UK, August 23–28, 2020, Proceedings, Part XIV 16*, pages 194–210. Springer, 2020. 3
- [29] Limeng Qiao, Wenjie Ding, Xi Qiu, and Chi Zhang. End-to-end vectorized hd-map construction with piecewise bezier curve. In *Proceedings of the IEEE/CVF Conference on Computer Vision and Pattern Recognition*, pages 13218–13228, 2023. 2, 7
- [30] Zequn Qin, Jingyu Chen, Chao Chen, Xiaozhi Chen, and Xi Li. Unifusion: Unified multi-view fusion transformer for spatial-temporal representation in bird’s-eye-view. In *Proceedings of the IEEE/CVF International Conference on Computer Vision*, pages 8690–8699, 2023. 1
- [31] Tixiao Shan and Brendan Englot. Lego-loam: Lightweight and ground-optimized lidar odometry and mapping on variable terrain. In *2018 IEEE/RSJ International Conference on Intelligent Robots and Systems (IROS)*, pages 4758–4765. IEEE, 2018. 1
- [32] Shihao Wang, Yingfei Liu, Tiancai Wang, Ying Li, and Xiangyu Zhang. Exploring object-centric temporal modeling for efficient multi-view 3d object detection. *arXiv preprint arXiv:2303.11926*, 2023. 1, 2
- [33] Shuo Wang, Xinhai Zhao, Hai-Ming Xu, Zehui Chen, Dameng Yu, Jiahao Chang, Zhen Yang, and Feng Zhao. Towards domain generalization for multi-view 3d object detection in bird-eye-view. In *Proceedings of the IEEE/CVF Conference on Computer Vision and Pattern Recognition*, pages 13333–13342, 2023. 1
- [34] Yingjie Wang, Qiuyu Mao, Hanqi Zhu, Jiajun Deng, Yu Zhang, Jianmin Ji, Houqiang Li, and Yanyong Zhang. Multi-modal 3d object detection in autonomous driving: a survey. *International Journal of Computer Vision*, pages 1–31, 2023. 1
- [35] Benjamin Wilson, William Qi, Tanmay Agarwal, John Lambert, Jagjeet Singh, Siddhesh Khandelwal, Bowen Pan, Ratnesh Kumar, Andrew Hartnett, Jhony Kaesemodel Pontes, et al. Argoverse 2: Next generation datasets for self-driving perception and forecasting. *arXiv preprint arXiv:2301.00493*, 2023. 6, 7
- [36] Dongming Wu, Fan Jia, Jiahao Chang, Zhuoling Li, Jianjian Sun, Chunrui Han, Shuailin Li, Yingfei Liu, Zheng Ge, and Tiancai Wang. The 1st-place solution for cvpr 2023 openlane topology in autonomous driving challenge. *arXiv preprint arXiv:2306.09590*, 2023. 1
- [37] Chenyu Yang, Yuntao Chen, Hao Tian, Chenxin Tao, Xizhou Zhu, Zhaoxiang Zhang, Gao Huang, Hongyang Li, Yu Qiao, Lewei Lu, et al. Bevformer v2: Adapting modern image backbones to bird’s-eye-view recognition via perspective supervision. In *Proceedings of the IEEE/CVF Conference on Computer Vision and Pattern Recognition*, pages 17830–17839, 2023. 2
- [38] Tianyuan Yuan, Yicheng Liu, Yue Wang, Yilun Wang, and Hang Zhao. Streammapnet: Streaming mapping network for vectorized online hd map construction. *arXiv preprint arXiv:2308.12570*, 2023. 1, 2, 5, 6, 7, 8
- [39] Ekim Yurtsever, Jacob Lambert, Alexander Carballo, and Kazuya Takeda. A survey of autonomous driving: Common practices and emerging technologies. *IEEE access*, 8:58443–58469, 2020. 1
- [40] Hao Zhang, Feng Li, Shilong Liu, Lei Zhang, Hang Su, Jun Zhu, Lionel M Ni, and Heung-Yeung Shum. Dino: Detr with improved denoising anchor boxes for end-to-end object detection. *arXiv preprint arXiv:2203.03605*, 2022. 3
- [41] Ji Zhang and Sanjiv Singh. Loam: Lidar odometry and mapping in real-time. In *Robotics: Science and systems*, pages 1–9. Berkeley, CA, 2014. 1
- [42] Yunpeng Zhang, Zheng Zhu, Wenzhao Zheng, Junjie Huang, Guan Huang, Jie Zhou, and Jiwen Lu. Beverse: Unified perception and prediction in birds-eye-view for vision-centric autonomous driving. *arXiv preprint arXiv:2205.09743*, 2022. 1
- [43] Xizhou Zhu, Weijie Su, Lewei Lu, Bin Li, Xiaogang Wang, and Jifeng Dai. Deformable detr: Deformable transformers for end-to-end object detection. *arXiv preprint arXiv:2010.04159*, 2020. 1, 4